Complete β-decay patterns of ^{142}Cs, ^{142}Ba, and ^{142}La determined using total absorption spectroscopy

M. Wolińska-Cichocka[1,2,3,*] B. C. Rasco,[2,3,4] K. P. Rykaczewski,[2] N. T. Brewer,[2,3,4] A. Fijałkowska,[5,4] M. Karny,[5,2,3]
R. K. Grzywacz,[2,3,4] K. C. Goetz,[6,4] C. J. Gross,[2] D. W. Stracener,[2] E. F. Zganjar,[7] J. C. Batchelder,[8,9] J. C. Blackmon,[7]
S. Go,[4,10] B. Heffron,[4] J. Johnson,[2,†] T. T. King,[2,4] J. T. Matta,[2,3] K. Miernik,[2,5] M. Madurga,[4] E. A. McCutchan,[11]
D. Miller,[4,12] C. D. Nesaraja,[2] S. V. Paulauskas,[4] M. M. Rajabali,[13] S. Taylor,[4] A. A. Sonzogni,[11] E. H. Wang,[14]
J. A. Winger,[15] Y. Xiao,[4,15] and C. J. Zachary[14]

[1]*Heavy Ion Laboratory, University of Warsaw, PL-02-093 Warszawa, Poland*
[2]*Physics Division, Oak Ridge National Laboratory, Oak Ridge, Tennessee 37831, USA*
[3]*JINPA, Oak Ridge National Laboratory, Oak Ridge, Tennessee 37831, USA*
[4]*Department of Physics and Astronomy, University of Tennessee, Knoxville, Tennessee 37966, USA*
[5]*Faculty of Physics, University of Warsaw, Pasteura 5, PL-02-093 Warszawa, Poland*
[6]*Nuclear and Extreme Environments Measurement Group, Oak Ridge National Laboratory, Oak Ridge, Tennessee 37831, USA*
[7]*Department of Physics and Astronomy, Louisiana State University, Baton Rouge, Louisiana 70803 USA*
[8]*Oak Ridge Institute of Science and Education, Oak Ridge, Tennessee 37831, USA*
[9]*Department of Nuclear Engineering, University of California, Berkeley, California 94720, USA*
[10]*RIKEN Nishina Center, Wako, Saitama, 351-0198, Japan*
[11]*National Nuclear Data Center, Brookhaven National Laboratory, Upton, New York 11973, USA*
[12]*SkuTek Instrumentation, West Henrietta, New York 14586, USA*
[13]*Department of Physics, Tennessee Technological University, Cookeville, Tennessee 38505, USA*
[14]*Department of Physics and Astronomy, Vanderbilt University, Nashville, Tennessee 37212, USA*
[15]*Department of Physics and Astronomy, Mississippi State University, Mississippi State, Mississippi 39762, USA*

Background: The β decays of fission products produced in nuclear fuel are important for nuclear energy applications and fundamental science of reactor antineutrinos. In particular, nuclear reactor safety is related to the decay modes of radioactive neutron-rich nuclei, primarily via the emission of γ rays, neutrons, and electrons. Additionally nuclear reactors are the most powerful man-made source of antineutrinos emitted during the β decay of fission products. These antineutrinos are used to inspect fundamental properties of leptons as well as informing reactor operation. However, the majority of data on complex decays of fission products collected in the evaluated nuclear data repositories like Evaluated Nuclear Structure Data File (ENSDF) and Evaluated Nuclear Data Files (ENDF) are based on low-efficiency and often incomplete measurements resulting in questionable reference reactor antineutrino flux predictions, see the analysis by [Nichols, J. Nucl. Sci. Technol. **52**, 17 (2015)]. Various assessments like the one done under the auspices of the [Yoshida *et al., Assessment of Fission Product Decay Data for Decay Heat Calculations: A report by the Working Party on International Evaluation Co-operation of the Nuclear Energy Agency Nuclear Science Committee* (Nuclear Energy Agency, Organization for Economic Co-operation and Development, Paris, France, 2007), Vol. 25], as well as by [Sonzogni, Johnson, and McCutchan, Phys. Rev. C **91**, 011301(R) (2015)] and [Dwyer and Langford, Phys. Rev. Lett. **114**, 012502 (2015)], list the $A = 142$ isobars with high cumulative fission yield among the important nuclei where data for reactor decay heat and/or antineutrino production should be verified and/or improved.

Purpose: Our goal is to improve the quality of β-decay measurements and evaluate the impact of modified decay schemes on reactor decay heat and antineutrino energy spectra, for fission products along the $A = 142$ isobaric chain. This work is an in depth follow-up on [Rasco *et al.,* Phys. Rev. Lett. **117**, 092501 (2016)]. which presented briefly the impact of the corrected decay scheme of ^{142}Cs. Here, we extend the data to full isobaric decay chain including the daughter nuclei, ^{142}Ba and ^{142}La, and present more details on the ^{142}Cs results.

Method: The decays of neutron-rich isobars of mass $A = 142$ produced by means of proton-induced fission of ^{238}U were measured using the Modular Total Absorption Spectrometer (MTAS) array on-line at the mass separator and Tandem accelerator at Oak Ridge National Laboratory.

Results: The β-decay schemes for ^{142}Cs and ^{142}La were modified with respect to the nuclear data repositories. A small β-delayed neutron branching ratio for ^{142}Cs emitter was remeasured as 0.10^{+5}_{-3} %. Improved precision on the measured half-lives is reported. Small corrections to the low-energy decay of ^{142}Ba are made. The β-decay

*mala@slcj.uw.edu.pl
†Deceased.

patterns for ^{142}La and ^{142}Cs are presented. The decay heat release and cross section for the detection of reactor antineutrinos are deduced and compared to earlier results.

Conclusions: The β-feeding pattern for ^{142}Cs having decay energy value Q_β of over 7 MeV was substantially modified with respect to the current ENSDF entry. Smaller changes were encountered for ^{142}La, but since this $A = 142$ isobar also has a large cumulative yield in fission, the changes influence both decay heat and the antineutrino spectra. The previously known β intensities for ^{142}Ba decay (Q_β value of 2.2 MeV) were verified and slightly modified. Overall, increased decay heat values and lower flux of antineutrinos interacting with matter are presented.

I. INTRODUCTION

According to the Power Reactor Information System (PRIS) of the International Atomic Energy Agency (IAEA), there were 422 nuclear reactors operating in the world at the end of 2022, with a total installed capacity of about 380 GW. Over 50 new power reactors are currently under construction which will add an additional 59 GW capacity in the coming years [1]. Power reactors provide about 10% of world-wide energy production producing about 30% of all low-carbon electricity [1] and as adaptable electric energy sources they played an important role during COVID-19 pandemic [2]. Therefore reliable data for the safety and efficiency of reactor operation, including the decay properties of fission products created in nuclear fuel, are critical for users of nuclear power all over the world.

Nuclear reactors are the most powerful sources of man-made antineutrinos and contribute to fundamental particle physics measurements. Reactor based neutrino oscillations experiments [3–5] and possible new generations of sterile neutrinos [6] are among hot topics in lepton physics. Next generation antineutrino experiments such as JUNO-TAO [7] that will measure precise antineutrino energies aiming for the detailed structure in the energy spectra (see Ref. [8]) and relate the results to the neutrino mass hierarchy [3,9]. These studies require reference reactor antineutrino flux to be determined with a precision better than 1%. Together with the experiments at research reactors, such as PROSPECT [10,11], MTAS-based investigations of antineutrino energy spectra help verify and improve data bases allowing experimental determination of the reaction operation properties for nonproliferation diagnostics [12].

Last but not least, the reliable determination of β-strength patterns is important for theoretical analysis of β-decay processes and allows prediction of post β-decay modes helping nuclear structure and nuclear astrophysics studies.

Our program of β-decay measurements of fission products resulted in precision measurements using total absorption methods [13–17]. Here, we report on the experiment and analysis details, derive β-decay properties and conclude on the β-γ emission along the $A = 142$ decay chain. The $A = 142$ isobars have cumulative fission yields at the level of 5% and were cited in the assessments [18–21] listing the most important fission products to be restudied with a total γ absorption method.

The results on the simultaneously measured activities in the $A = 142$ decay chain serve as an example of the impact of total gamma absorption measurements for nuclei with β-decay energy Q values spanning from 2.2 MeV for ^{142}Ba up to 7.3 MeV for ^{142}Cs. With increasing β-decay energy many weak β transitions populate states in a region with high level density in the daughter nucleus and are followed by cascades of weak and often high-energy γ rays. These γ transitions often remain undetected during low-efficiency measurements. This effect is usually referred to as a "pandemonium effect" following the work of Hardy *et al.* [22]. The total absorption spectrometry (TAS) of γ radiation was recognized as an antipandemonium technique demonstrated by Duke and others [23], operating two NaI(Tl) crystals surrounding at he derivation measured radioactive sample. Several TAS devices were constructed and used in β-decay studies in the following years [24–33]. The recent review [34] points to the importance of TAS measurement allowing the derivation of true β-strength distributions and their consequences. The world largest and most efficient array, the Modular Total Absorption Spectrometer (MTAS) was designed, constructed, and commissioned at the Holifield Radioactive Ion Beam Facility (HRIBF) at Oak Ridge National Laboratory (ORNL) to perform total gamma absorption measurements of complex β decays, in particular of fission products [13,14,35–39]. The MTAS segmentation facilitates reliable analysis of the decay patterns involving several cascading γ rays and ground state feeding [15–17].

The $A = 142$ decay chain includes the short-lived ^{142}Cs isotope ($T_{1/2} = 1.68$ s, $Q_\beta = 7.33$ MeV). The ^{142}Cs activity decays to even-even ^{142}Ba ($T_{1/2} = 10.6$ min, $Q_\beta = 2.18$ MeV), and it is followed by the decay of odd-odd ^{142}La ($T_{1/2} = 91.1$ min, $Q_\beta = 4.51$ MeV) to the practically stable isotope ^{142}Ce.

The β decays of ^{142}Cs, ^{142}Ba, and ^{142}La were previously studied, mostly using the high energy resolution but low-efficiency counting methods [40–42]. The decays of ^{142}Ba $\rightarrow$ ^{142}La and ^{142}La $\rightarrow$ ^{142}Ca also were measured with an early total absorption gamma spectrometer [43]. The present MTAS results also include the ^{142}Cs β-delayed neutron branching ratio, determined in this work to be 0.10^{+5}_{-3} %. Verified and expanded data on the ^{142}Ba and ^{142}La decays is reported. The ^{142}Cs activity is among the top three components of the high-energy part of the reactor antineutrino spectra [20,21] and contributes to the decay heat and to the β-delayed neutron emission at short times after fission event [13,14]. The difference between β-feeding values obtained from MTAS measurement and Evaluated Nuclear Structure Data File (ENSDF) database for all three nuclei confirms the
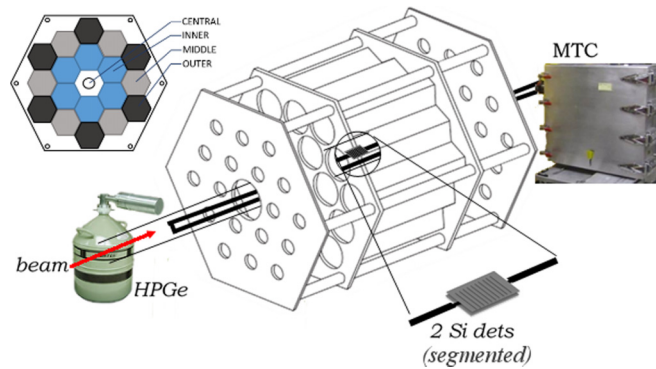
FIG. 1. A schematic view of HRIBF Modular Total Absorption Spectrometer (MTAS), auxiliary Si-strip detectors (40 mm × 60 mm), monitoring Ge counter and tape drive operating with MTAS (not to scale). Inlet shows modular construction of MTAS array includes three rings of NaI(Tl) detectors referred to as the inner, middle and outer ring, depending on the module distance from the center of the array.

unique capabilities of total gamma absorption measurements, particularly for nuclei with high-Q_β values.

II. EXPERIMENTAL DETAILS

The Modular Total Absorption Spectrometer (MTAS) array [35,37,38] was designed, constructed, characterized, commissioned and used in the decay studies of ^{238}U fission products at the ORNL's HRIBF [44]. 5 to 50 nA 40 MeV proton beams from the ORNL Tandem induced fission in a UCx (uranium carbide) target that was close-coupled to an ion source [45] of the on-line mass separator. For the $A = 142$ decay chain nuclei, the ion source emits positive ions directly from a hot tantalum surface. This type of ion source has a high ionization efficiency for group 1 elements (e.g., Rb and Cs) and significantly lower efficiency for group 2 (e.g., Sr and Ba) and group 13 (e.g., Ga and In). The ionization efficiency for all other elements is practically zero. The tantalum ionizer was 30 mm long with an internal diameter (ID) of 3 mm. The beam of $A = 142$ from the surface ion source was extracted and analyzed by the on-line mass separator with a mass resolution as $m/\Delta m = 600$. Radioactive beams were deposited on the movable tape of the moving tape collector (MTC) and periodically moved into the MTAS (see example in Sec. III B). An HPGe detector was used to monitor the radioactive sample during the collection. The collect-wait-move-measure-move-move cycle times were adjusted according to the half-lives of the measured activities. Two tape moves after the measurement were used to move the radioactive sample into the shielded chamber of the MTC. The MTAS detector array, shown in Fig. 1, with its modular construction, consists of 19 NaI(Tl) hexagon-shaped 53.34 cm long detectors and 17.6 cm wide (side-to-side). The central module has a 6.35 cm diameter through hole facilitating the MTC tape-implanted radioactivity movements along the tape ladder. The auxiliary detectors include two 1-mm-thick Si β-trigger counters, each divided into seven 8.5 mm wide strips segmented perpendicular the beam axis. These Si detectors are placed at the center of MTAS surrounding the tape transporting the activities. The Si-segmented structure helps to verify the measuring position and center the radioactive sample in the middle of MTAS. The electron energy deposits in the silicon detectors are used as a β trigger. The coincidence condition between silicon detectors and MTAS reduced background such as the 1461 keV ^{40}K γ line, by about three orders of magnitude. All signals are processed using digital signal processing electronics, Pixie16 modules, Rev.D [46,47].

The mass of NaI(Tl) in the MTAS array is nearly 1000 kg, it covers over 99% of the solid angle around the activities stopped in the center. The entire array was surrounded by over 5000 kg of lead and neutron shielding foam SWX 227A. This shielding reduces the laboratory γ background by at least two orders of magnitude. The background rate in the total MTAS singles spectrum (not gated by β signals) at the HRIBF was about 2400 Hz for an energy range up to 8 MeV. The γ-ray efficiency for full-energy deposition of a single γ-ray in on-line measurements conditions is about 81% at 300 keV and about 71% at 6 MeV [38], while the total efficiency (i.e., the efficiency of registering any fraction of the incoming γ-ray energy) is about 98.9% at 500 keV. The MTAS threshold for individual modules is about 25 keV for the 18 regular modules, while the threshold for the central module is around 30 keV. This slightly larger threshold in the central module is a combined effect of the light collection from the individual sections of the central module and of the different photomultipliers [37,38].

III. INITIAL ANALYSIS

A. MTAS raw spectra and data base driven simulations

A straight-forward analysis, often done on-line during the experiment, is to compare MTAS-measured β-gated total energy spectra with the simulations based on the current data base content. These comparisons are performed after the isobaric purification of the collected spectra. The spectra analysis times after each start of the cyclic measurements are selected according to the isobaric half-lives, and the subtraction of the shorter-lived and longer-lived components is performed (if appropriate). The respective comparisons for ^{142}La, ^{142}Ba, and ^{142}Cs decays are shown in Figs. 2–4. The input data for the simulations are based on the current ENSDF entries [48]. For ^{142}La and ^{142}Ba two simulations are presented, the high-energy resolution data are complemented by earlier TAS results from Greenwood *et al.* [43] included in ENSDF [48].

Differences are clearly visible for ^{142}Cs, while minimal changes to the decay schemes might be expected for ^{142}La and ^{142}Ba. However, the less obvious changes in the β-decay intensity patterns and their consequences are revealed after the full analysis of the experimental data.

B. Half-lives

The half-life $T_{1/2}$ is a basic decay property characterizing every radioactivity and is needed for simulations involving decay networks. Most MTAS high statistics measurements on fission products are particularly well suited to verify the half-lives used in reactor operations and neutron capture/decay
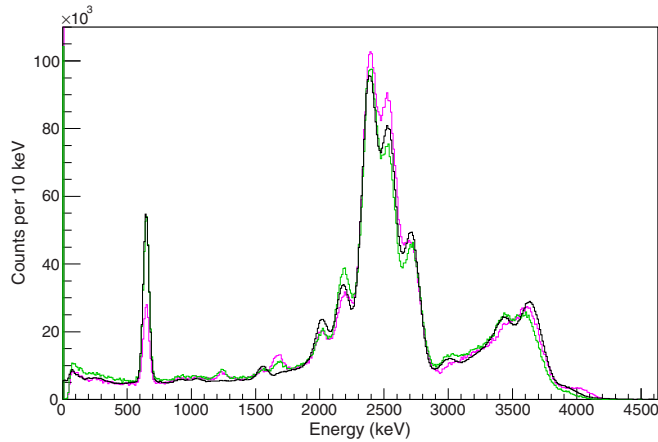
FIG. 2. ^{142}La $\rightarrow$ ^{142}Ca decay: comparison of MTAS data (black) to the simulated MTAS response calculated using the high-resolution spectroscopy results (pink) and Greenwood's [43] TAS results (green) listed in ENSDF [48].

FIG. 4. ^{142}Cs $\rightarrow$ ^{142}Ba decay: comparison of MTAS data (black) to the simulated MTAS response for the ENSDF entry [48] based on the high energy resolution data (cyan).

processes in astrophysical scenarios. In most cases, the half-life can be extracted without the full deconvolution of the measured MTAS spectra. This is the case for the $A = 142$ chain with very different half-lives for individual isobars. The simple analysis of measurements performed at different time frames and respective background subtractions allow us to obtain pure spectra associated with a particular activity. The summary of the cycle times and measurement patterns for $A = 142$ MTAS counting is given in Table I. No contaminating activities were detected. Figures 5–7 present the MTAS-measured $A = 142$ β-γ activities versus time.

The ^{142}La activity versus time with an exponential fit is shown in Fig. 5. To determine ^{142}La half-life we use the β-gated MTAS total energy events between 2.5 and 4.0 MeV to ensure there is minimal background contamination since all neighboring nuclei have $Q_\beta \lesssim 2500$ keV. Also, the fit range starts 40 minutes after the sample collection, to ensure
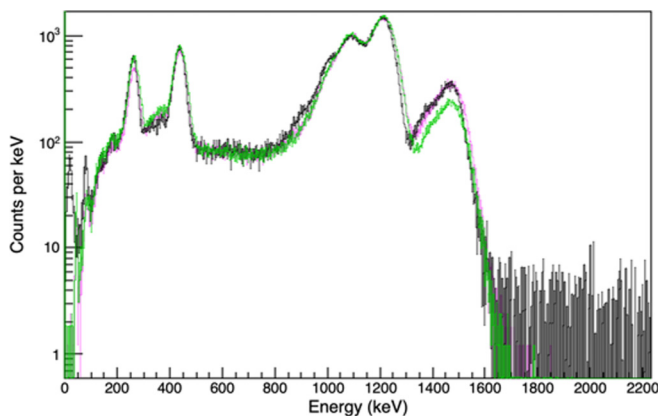
removal of the ^{142}Ba parent activity. For an exponential decay fit, we get a ^{142}La half-life of $T_{1/2} = 91.18(7)$ min. For the same data, using a decay model of a single exponential plus a constant background extracts $T_{1/2} = 91.3(1)$ min. We report the average of these two values yielding $T_{1/2} = 91.2(1)$ min, five times more precise than the current value listed at ENSDF [48], $T_{1/2} = 91.1(5)$ min, and also more precise than a recent measurement of 91.8(12) min [49].

To extract the ^{142}Ba half-life, we use the energies between 170 and 1570 keV to minimize background and set the counting time range after the sample movement between 60 and 240 s. The cut on the energy suppresses the contribution of the daughter, ^{142}La, since the majority of the ^{142}La decay results in a β-feeding above 2 MeV in its daughter ^{142}Ce. The fitting range starting 80 s after the sample collection and lasting 160 s removes the very short lived activity in the measured sample of the ^{142}Cs parent. The large uncertainty of the half-life is due to the short measurement time, which is shorter than the half-life of ^{142}Ba, and due to long-lived ^{142}La contribution. Using a decay model of a simple exponential we get ^{142}Ba $T_{1/2} = 10.5(4)$ min. However, when we use a Bateman decay model we get ^{142}Ba half-life of $T_{1/2} = 10.5(15)$ min, observing that the $T_{1/2}$ precision depends on the end points of the fit. The final quoted uncertainty of 1.5 min accounts for the uncertainty using the more accurate but less precise Bateman equation and is much larger than the 0.4 min for the single

FIG. 3. ^{142}Ba $\rightarrow$ ^{142}La decay: comparison of MTAS data (black) to the simulated MTAS response for ENSDF entry based on the high energy resolution data (pink) and to Greenwood's [43] TAS results (green) also listed in ENSDF [48]. The contribution of ^{142}La daughter activity to MTAS ^{142}Ba spectrum is subtracted in this figure.

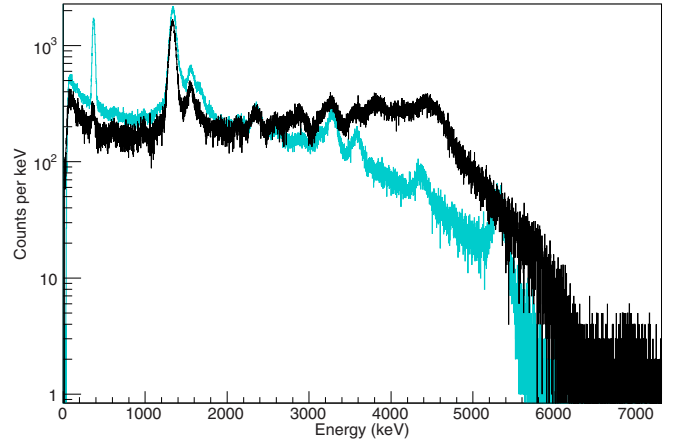TABLE I. The summary of the cycle times for $A = 142$ MTAS counting.

Isobar	collection	transport time	measurement
^{142}La	3600 s	60.78 s[a]	24 hours
^{142}Ba	60 s	60.78 s[a]	180 s
^{142}Cs	3.6 s	780 ms	5.1 s

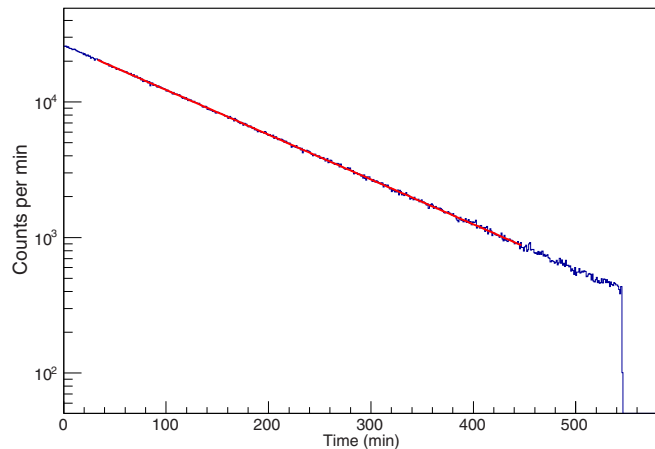[a]Includes 60 s waiting time after a sample collection, to reduce initial parent activity.

FIG. 5. The analyzed ^{142}La activity decay vs time determined using β-gated MTAS total energy events between 2.5 and 4 MeV (black). The result of a single exponential fit with no background component is given in red (see comments in text).

exponential fit. Our ^{142}Ba half-life match the ENSDF entry, $T_{1/2} = 10.6(2)$ min, though with less precision.

For the ^{142}Cs half-life, we used the spectrum measured 3 times longer then its half-life. The gate on total MTAS energy deposit was between 4 and 5 MeV to minimize background contamination. For a simple exponential decay model, we get ^{142}Cs $T_{1/2} = 1.678(8)$ Sec. This is in agreement within 1σ value with the ENSDF value of $T_{1/2} = 1.684(14)$ sec, but more precise. Our uncertainty is smaller due to large statistics and little to no background in the high-energy gate. The analyzed decay pattern for ^{142}Cs is shown in Fig. 7.

Our half-life results help confirm that clean spectra of the $A = 142$ isobars were obtained. When using the time patterns of the measurements and the energy range of MTAS signals adjusted to the individual isobars, we can improve the previously measured half-lives precision. The ENSDF entries on the ground state spin, parity, and half-lives are of studied activities are given in the Table II together with MTAS measured
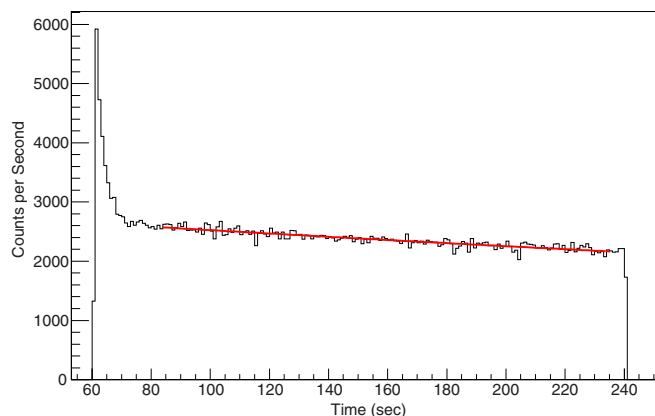

FIG. 6. The analyzed ^{142}Ba activity vs time obtained for the β-gated MTAS total energy events between 170 and 1570 keV (black). The result of a single exponential fit with no background component is given in red (compare text).
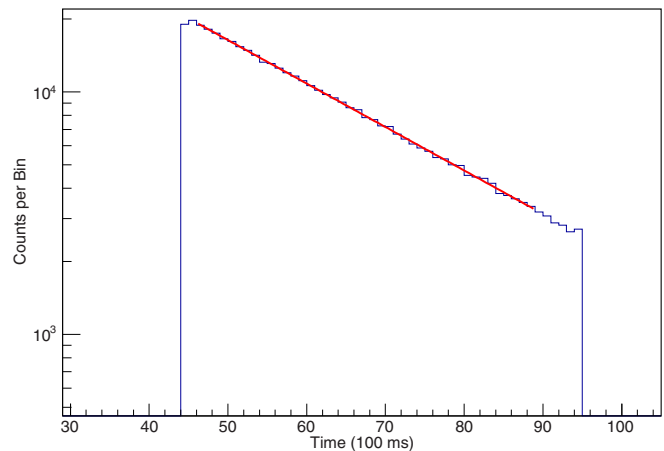

FIG. 7. The analyzed ^{142}Cs activity vs time for the β-gated MTAS total energy events between 4 and 5 MeV (black). The results of a single exponential fit with no background component is given in red. The results are insensitive within error bars to the variations of time range endpoints chosen for the fit (see text).

half-life values. The listed decay energies follow the recent assessment [50].

IV. ADVANCED ANALYSIS

A. Decay path determination with MTAS

The MTAS response function was established using off-line calibration γ and β sources, see Refs. [38,51], and a set of GEANT4 simulations [13–15,52] with MTAS and its auxiliary detectors included in the interactions of radiation with surrounding matter. The high-resolution data as well as MTAS-based analysis of individual decay paths are helpful for deriving the β-feeding patterns and the de-excitation γ cascades.

The modularity of MTAS allows us to determine the complex β-γ de-excitation paths [15,51,53]. Here, the technique is illustrated for the ^{142}La decay. If we make a gate on the total energy detected in MTAS for a given energy of a β-fed level, and then inspect the energy deposits in the center module, as shown in Fig. 8, and in the inner, middle and outer individual modules spectra, as in Fig. 9, we can identify individual energies of various γ rays in the daughter nucleus [15,51]. We simulate each set of de-excitation γ rays, or decay path, in GEANT4. This models the various γ-ray energy deposits in each MTAS module. Then we scale each decay path and

TABLE II. Decay properties $A = 142$ isobars.

Nuclei	Q_β [50]	GS Spin [48]	$T_{1/2}$ ENSDF	$T_{1/2}$ MTAS
^{142}Cs	7328(8) keV	0^-	1.684(14) s	1.678(8) s
^{142}Ba	2182(8) keV	0^+	10.6(2) min	10.5(15) min
^{142}La	4509(6) keV	2^-	91.1(5) min	91.2(1) min
^{142}Ce[a]		0^+	$>5 \times 10^{16}$ yr	

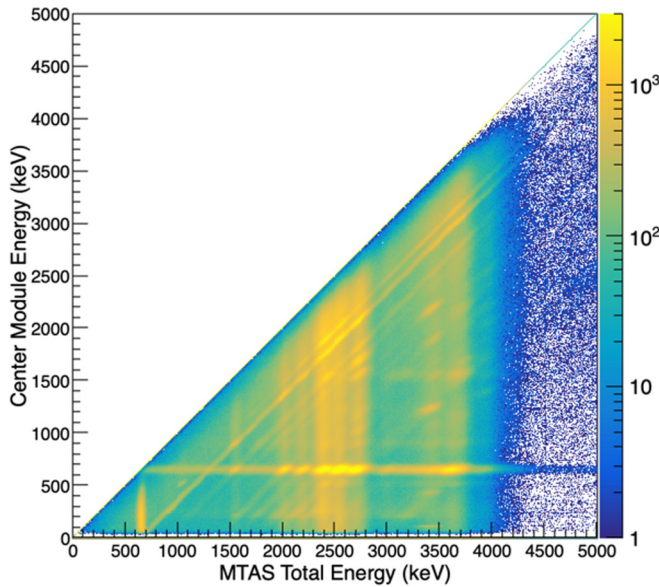[a]^{142}Ce can undergo a double β decay, it is stable against a single β decay.

FIG. 8. The coincidence data for ^{142}La decay. The center module energy is plotted versus the total MTAS energy spectrum. The z scale is logarithmic.

fit them to the measured spectrum. Due to the inability to separate nearby energy peaks, for each decay path with a different number of γ rays, the exact decay path determination is not always possible [16,17,43]. However, we establish the decay paths of γ-ray cascades from each bin and the energies of β-fed levels therein. This is illustrated by projecting the two-dimensional spectra presented in Figs. 8 and 9 gating at the total energies of between 3390 and 3430 keV. This projection is shown in Figs. 10 and 11. In Fig. 12, the energy
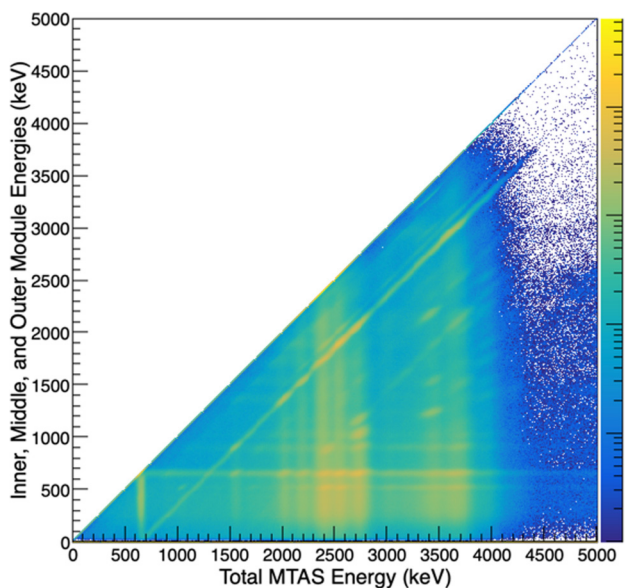

FIG. 9. The energy measured in the individual MTAS modules is plotted versus the total MTAS energy spectrum for ^{142}La data. The z scale is logarithmic.
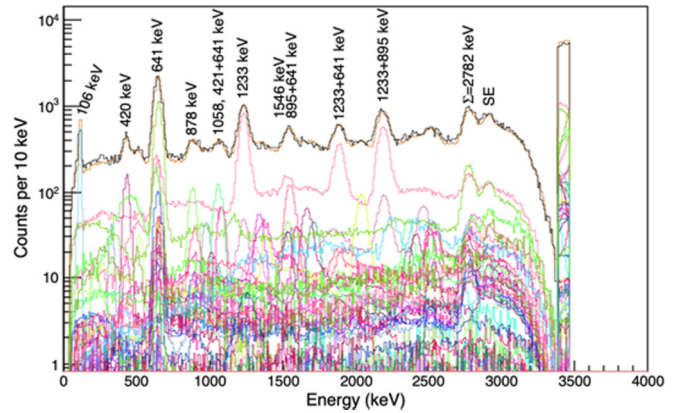

FIG. 10. Decay events of ^{142}La measured at the MTAS central (C) module gated by the MTAS total energy deposition between 3390 and 3470 keV. The experimental spectrum (black) and the total fit (orange) is displayed together with a simulation based on the high energy resolution data for the de-excitation of levels at 3420 and 3423 keV. All other color spectra represent various individual decay paths.

gate of 3420–3470 keV is shown for the center MTAS energy versus the total MTAS energy.

B. MTAS spectra deconvolution

Here, we present examples of the analysis steps leading to the interpretation of MTAS full energy spectrum. For illustration purposes, we present the MTAS response to a select few ^{142}La β-γ deexcitation paths in Fig. 13. The β feeding to the levels at 2004.3 and 641.3 keV and to the ground state marked in green, orange, and red, are followed by the respective γ deexcitations. The particular MTAS responses to these β and γ radiation are identified in Fig. 13. These particular decay paths can be identified in the full deconvolution shown in Fig. 14.

The full deconvolution of MTAS β-gated spectrum for the measured ^{142}La decay is presented in Fig, 14. The total
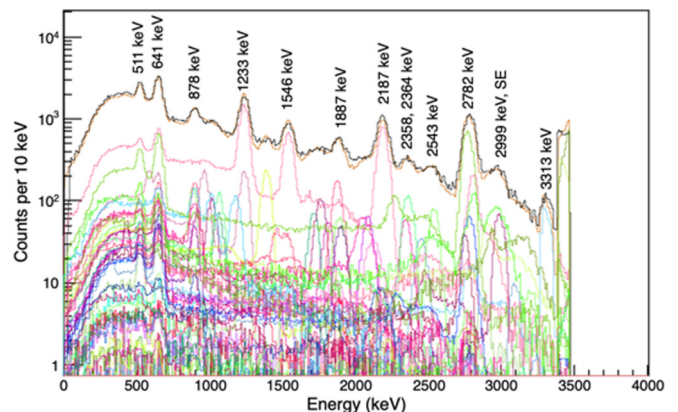
FIG. 11. Decay events of ^{142}La measured at the MTAS inner (I), middle (M), and outer (O) individual modules gated by the MTAS total energy deposition between 3390 and 3470 keV. The experimental spectrum (black) and the total fit (orange) is displayed together with a simulation based on the high energy resolution data for the de-excitation of levels at 3420 and 3423 keV. All other color spectra represent various individual decay paths.

FIG. 12. Decay events of ^{142}La measured at the MTAS central (C) module gated by the MTAS total energy deposition between 3420 and 3470 keV. The experimental spectrum (black) and the total fit (orange) is displayed together with a simulation based on the high energy resolution data for the de-excitation of levels at 3420 and 3423 keV. All other color spectra represent various individual decay paths.
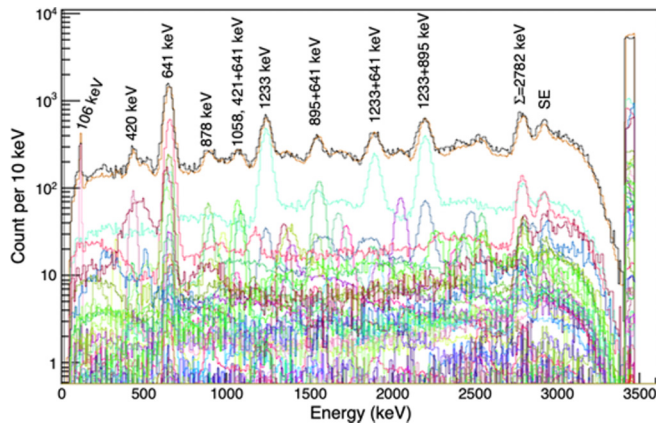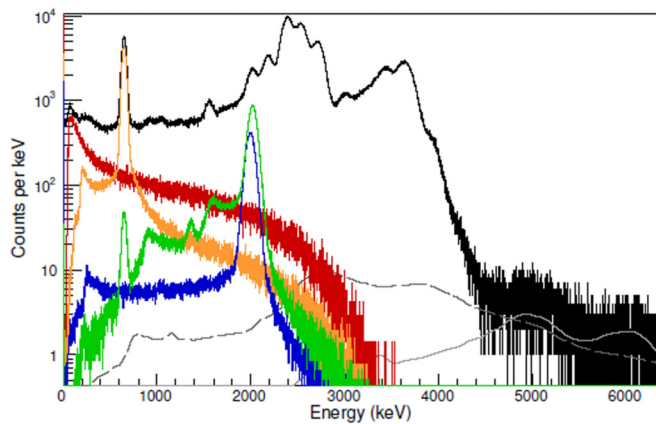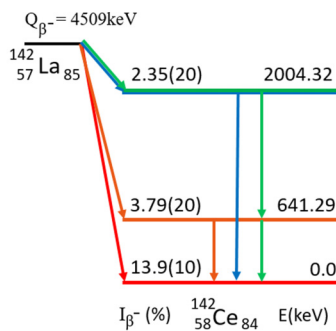

FIG. 13. Upper panel: The partial decay scheme of ^{142}La with selected decay paths marked by color. Lower panel: MTAS total energy spectrum for ^{142}La decay gated by β signals is given in black. Some components contributing to this MTAS spectrum and indicated in the upper panel are plotted: red - the ground-state to ground-state feeding response, orange - β decay to the 1st excited state which deexites via a single 641 keV, blue - β decay to the 2004 keV level followed by a single 2004 keV γ decay path, green - β decay to the 2004 keV level followed by two γ rays cascade (1363 and 641 keV γs), grey - the pileup events, dashed gray - the events which are coincident with the background
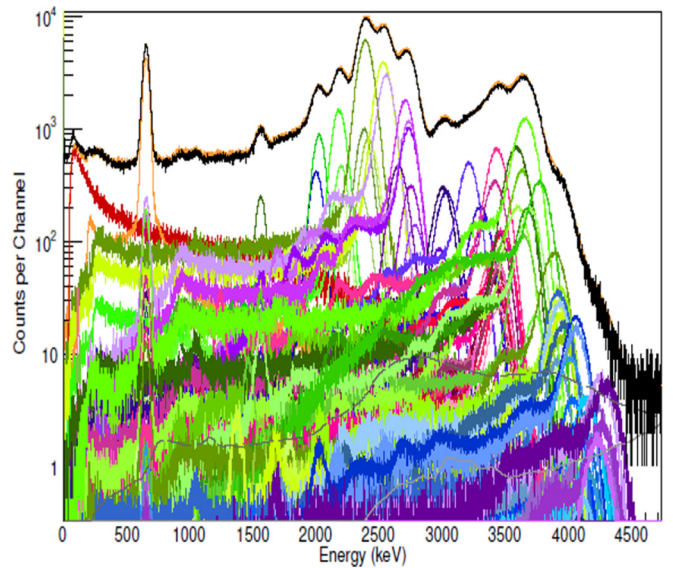

FIG. 14. Complete deconvolution of MTAS-measured energy spectrum following ^{142}La β decay. Fit of the simulated MTAS response functions for individual decay paths (multicolored) to the MTAS data (black) are presented. The sum of the fit of all of the response functions is shown in orange and overlaps well with MTAS experimental result (black). Pileup and background coincidences, which contribute counts above the Q_β energy of 4509 keV, are shown in grey (barely visible). The pileup and background coincidences account for less than $\approx 0.7\%$ of the total number of counts. The relative fit of the response functions is also based on gating the total MTAS energy while looking at the individual module responses.

MTAS spectrum is well reproduced by the multicomponent fit involving 38 β-decay paths listed at the ENSDF and the following γ rays.

FIG. 15. De-convolution of MTAS-measured energy spectrum following ^{142}Ba β decay. Fit of the simulated MTAS response functions for individual decay paths (multicolored) to the MTAS data (black). The sum of the fit of all of the response functions is shown in orange. Pileup and background coincidences, which contribute counts above the Q_β energy, are shown in dark green. The relative fit of the response functions is also based on gating the total MTAS energy while looking at the individual module responses.
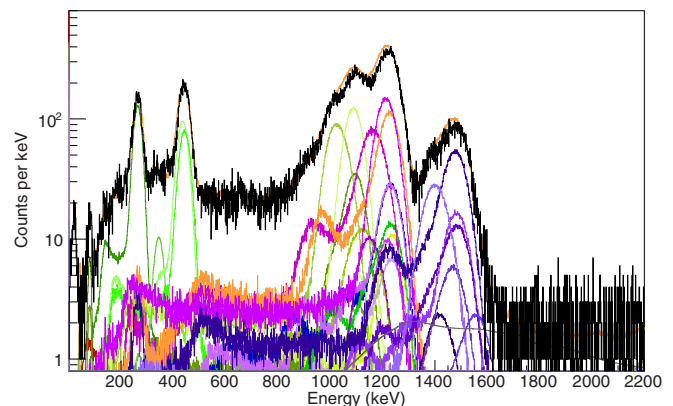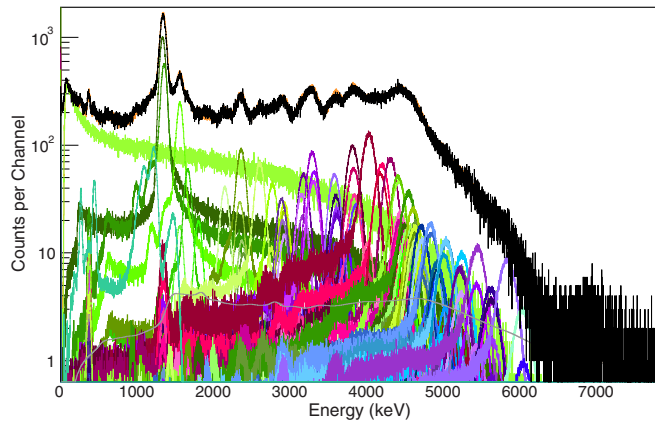
FIG. 16. Deconvolution of MTAS-measured energy spectrum following ^{142}Cs decay. Fit of the simulated MTAS response functions for individual decay paths (multi-colored) to the MTAS data (black). The sum of the fit of all of the response functions is shown in orange. Background coincidences, which contribute counts above the Q_β energy, are shown in gray. The relative fit of the response functions is also based on gating the total MTAS energy while looking at the individual module responses. The peak near 6900 keV is from the small β-delayed neutron branch.

The full deconvolution of the ^{142}Ba and ^{142}Cs decays measured by MTAS are given in Figs. 15 and 16, while the derived β and γ intensity distributions are listed in the Appendix. As mentioned above, the fits result not only from the response function for the total MTAS energy spectra as shown in Figs 2–4 but also from gating on the total MTAS energy and fitting the response functions for each module.

V. MAIN RESULTS

A. Deduced β-feeding patterns in ^{142}La decay

The main differences between MTAS and earlier high-energy resolution and Greenwood TAS results [43] are visible in Fig. 2 and are quantified after the full deconvolution. The spread of β-intensities between the MTAS, ENSDF, and Greenwood data can be clearly seen in the β-feeding intensity to the ^{142}Ce ground state and to the first excited state at 641 keV. The ground-state to ground-state transition is a first forbidden unique decay, $2^- \to 0^+$, and the $2^- \to 2^+$ β transition to the first excited state is first forbidden nonunique

TABLE III. The ^{142}La $\to$ ^{142}Ca β-decay intensities I_β from the 2^- ground state to the 0^+ ground state and from the 2^- ground state to the 2^+ first excited state at 641 keV obtained by Tong *et al.* [40], by Greenwood *et al.* [43] listed in the current mass $A = 142$ ENSDF evaluation [48] and our MTAS results.

	gs to gs feeding	gs to 2$^+$ excited state
Tong	10.8^a %	13.8^a %
ENSDF	16.5 ± 1.0%	1.4 ± 0.4%
Greenwood	21.0 ± 2.5%	3.5^a %
MTAS	14.0 ± 1.0%	3.7 ± 0.2%

^{a}No uncertainties given in the original paper.
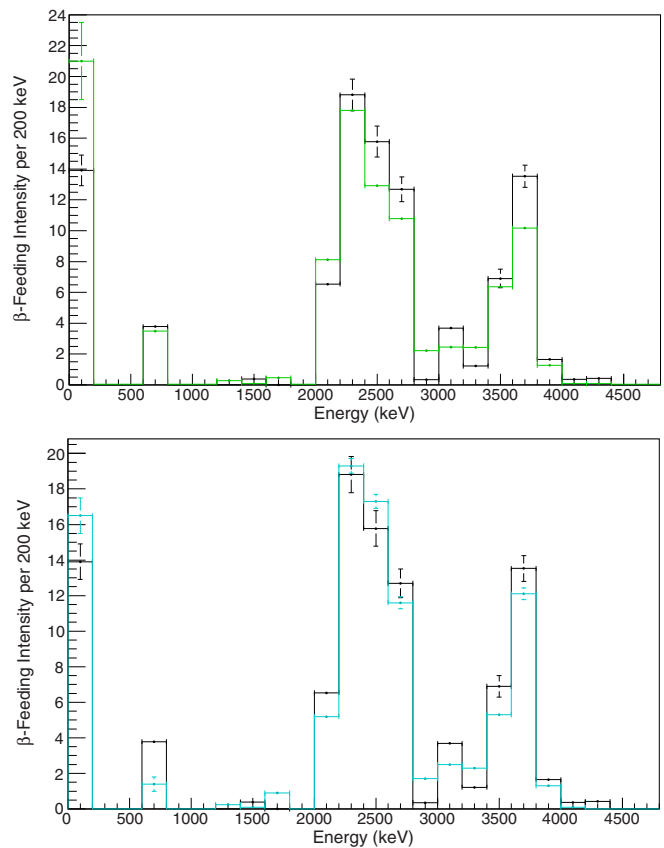
FIG. 17. (Top) MTAS β-feeding intensities (black) compared with the Greenwood β-feeding intensities (green) for the β decay of ^{142}La. The Greenwood data offers an uncertainty only for the ground-state to ground-state feeding. (Bottom) MTAS β-feeding intensities (black) compared with the ENSDF β-feeding intensities (cyan) for the β decay of ^{142}La [48].

transition. The intensities for these β transitions are compared in Table III. For the ground state to ground state β transition, we also show the previous result from Tong *et al.* [40] and Greenwood *et al.* [43] as well as the evaluated ENSDF entry.
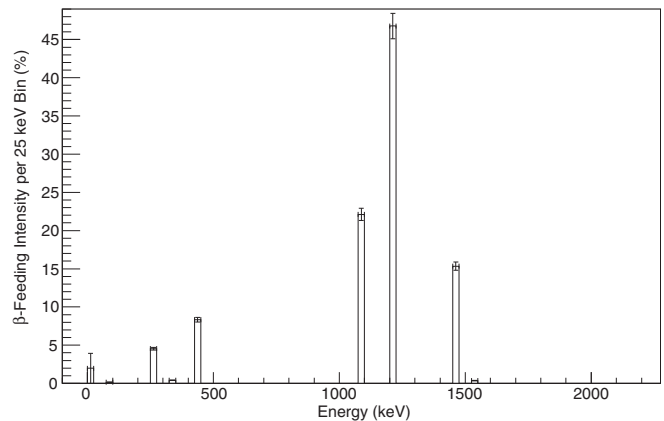
FIG. 18. ^{142}Ba $\to$ ^{142}La MTAS β-feeding intensities per 25 keV. The results are similar within experimental uncertainties with the ENSDF and Greenwood data.
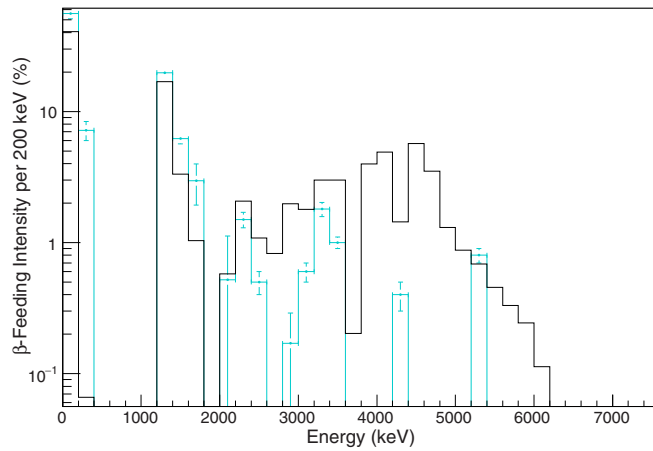
FIG. 19. ^{142}Cs MTAS β-feeding (black) intensities per 200 keV compared to the ENSDF (cyan) data [48].

The main discrepancy is identified as the β-feeding to the first excited 2^+ state in ^{142}Ce. Greenwood *et al.* [43] and MTAS data show consistent results, a two times higher β-transition intensity to this lowest excited state, when compared with the ENSDF entry [48]. Tong *et al.* [40] reported a value of about four times higher intensity as compared to the total absorption measurements. Typically, the TAS-technique redistributes the β-transition probabilities measured with high energy resolution detectors but low efficiency techniques, by increasing the feeding to higher excited states at the cost of reducing β-transition intensities to low-energy states.

The full β-feeding pattern of ^{142}La decay resulting from the MTAS measurement is listed in the Table VII together with the ENSDF high energy resolution results and TAS entries. The β-feeding intensities derived using MTAS data are shown in Fig. 17.

B. Deduced β feeding patterns in ^{142}Ba decay

The small differences between MTAS and the simulated response of MTAS for the ENSDF ^{142}Ba decay data are presented in Fig. 3. The counts above 1.8 MeV are dominated by decays from the daughter, ^{142}La. The data are normalized to the same number of counts between 1 and 6500 keV. For this

TABLE IV. The fission cumulative yields (in percents) for $A = 142$ isobars for ^{235}U, ^{239}Pu and ^{241}Pu for thermal neutrons and ^{238}U for 500 keV neutrons based on ENDF data [54,55] and JEFF data base [56].

Nuclei	Ref.	Fission cumulative yields (%)			
		^{235}U	^{238}U	^{239}Pu	^{241}Pu
^{142}Cs	[54,55]	2.717(76)	3.85(62)	1.54(25)	3.24(75)
	[56,57]	3.02(26)	4.35(19)	1.56(27)	2.74(19)
^{142}Ba	[54,55]	5.75(12)	4.58(18)	4.63(37)	4.71(19)
	[56,57]	5.812(76)	4.84(21)	4.802(56)	4.45(14)
^{142}La	[54,55]	5.849(82)	4.586(92)	4.925(35)	4.747(95)
	[56,57]	5.843(76)	4.84(21)	4.959(5.5)	4.48(14)

TABLE V. Average gamma energy per decay $\langle E_\gamma \rangle$ (in keV) for ^{142}Cs, ^{142}Ba, ^{142}La decays, from MTAS and earlier data.

Nuclei	MTAS	ENSDF	Greenwood[a]
^{142}La	2350 ± 200	2290 ± 150	2120
^{142}Ba	1015 ± 30	1100 ± 50	1058
^{142}Cs	1760 ± 50	670 ± 40	

[a] No uncertainties given in the original work.

relatively low β-decay energy value of $Q_\beta = 2182(8)$ keV our measurements are in general agreement with earlier data coming from the high-resolution detectors as well as previous total absorption gamma spectroscopy measurements [43].

The ground state feeding should be treated as an upper bound due to the extremely small number of counts that could come from any small contamination and the small total MTAS efficiency of the ground-state to ground-state response function, which is about 2.9%, i.e., only 2.9% of ground state events leave some energy in MTAS, almost all of which is from Bremsstrahlung. The $<4\%$ feeding to the ground state dominates the uncertainties for most other levels besides the small β-fed levels. Uncertainty on the 78 keV level is dominated by the conversion electron coefficient (α) and its uncertainty, $\alpha = 3.6 \pm 1.4$ [48]. The 78-keV γ is clearly visible in the total MTAS spectrum and is larger than the expected number of partially detected decays from other levels that decay through the 78-keV level.

The comparison between current and earlier data on the β-feeding intensity pattern is also given in Appendix. The extracted MTAS β-feeding intensities are presented in Fig. 18 and Table VI.

TABLE VI. β-feeding intensities I_β listed at ENSDF [48] for high energy resolution studies and TAS-technique measurement by Greenwood *et al.* [43] compared to MTAS data for ^{142}Ba $\rightarrow$ ^{142}La decay.

E_{level} [keV]	I_β (%) ENSDF[a]	I_β (%) Greenwood[b]	I_β (%) MTAS
0		} 2.0 (1.9)	<4
78			0.15(5)
225.3	3.5 (7)	4.6	4.5(2)
335.0	0.3 (1)	0.3	0.4(1)
425.0	5.4 (2)	6.0	} 8.3(3)
432.0	4.3 (2)	4.8	
1078.7	22 (1)	22	22.1(8)
1204.3	46 (2)	46	46.8(17)
1457.9	15.4 (6)	14	15.3(6)
1539.3	0.28 (5)	0.28	0.4(1)

[a] Ground state to ground state β intensity of $\sim$2% guided by Greenwood result [43] is included at the ENSDF normalization of total β feeding.

[b] Except for ground state to ground state transition no uncertainties given in the original work.

TABLE VII. β-feeding intensities in the ^{142}La $\rightarrow$ ^{142}Ca obtained in this work (MTAS) are compared to the respective ENSDF entries [48] obtained with high energy resolution methods as well as to the measurements performed with TAS technique by Greenwood *et al.* [43]. $< E_{bin} >$ represents the center of the ^{142}Ce excitation energy bin taken into account during MTAS data analysis. The bin width was set to 25 keV up to the last known level (4050 keV) and to 50 keV for levels above 4050 keV.

E_{level} (keV)	I_β (%) ENSDF	I_β (%) Greenwood[a]	E_{level} (keV)	$< E_{bin} >$ MTAS	I_β (%)
0	16.5 (10)	21.0(25)	0	0	13.9(10)
641	1.4 (4)	3.50	641	650	3.79(20)
1219	0.24 (10)	0.28	1219	1225	0
1536	≈0.1	≈0.09	1536	1525	0.4(2)
1653	0.9 (2)	0.46	1653	1650	0
2004	1.6 (1)	1.48	2004	2000	2.35(20)
2015		0.55	2015	} 2025	} 0.04(4)
2031		0.55	2031		
2044		0.55	2044	2050	
2182	0.4 (1)	0.55	2182	} 2175	} 4.15(20)
2187	3.2 (2)	4.43	2187		
2365	1.5 (1)	1.38	2365	2375	2.7(2)
2398	17.8 (4)	16.41	2398	2400	16.1(10)
2543	17.3 (4)	12.91	2543	2550	15.8(10)
			2575	2575	0
			2650	2650	1.183(50)
2667	3.1 (2)	1.38	2667	2675	10.7(8)
2697	6.7 (2)	7.41	2697	2700	0
2727	0.6 (1)	0.66	2727	2725	0.81(8)
2742	0.9 (1)	1.00	2742	2750	0
2767	0.3 (1)	0.33	2767	2775	0
2801	0.9 (1)	0.66	2801	2800	0.338(50)
2999	0.8 (1)	1.57	2999	3000	1.03(10)
3061	0.8 (1)	0.74	3061	3050	0.893(80)
3154	0.7 (1)	0.71	3154	3150	1.92(15)
3181	1.0 (1)	1.01	3181	3200	0
3304	1.0 (1)	1.06	3304	} 3300	} 1.00(12)
3313	1.3 (1)	1.38	3313		
3420	2.1 (1)	2.52	3420	} 3425	} 6.19(60)
3423	1.2 (1)	1.44	3423		
3460	1.2 (1)	1.44	3460	} 3450	} 0.724(70)
3470	0.8 (1)	0.96	3470		
3612	5.0 (1)	4.61	3612	3600	2.69(20)
3633	1.7 (1)	1.57	3633	3625	} 3.16(30)
3648	1.1 (1)	1.01	3648	3650	
3676	1.2 (1)	0.83	3676	} 3675	} 6.06(60)
3689	0.5 (1)	0.35	3689		
3704	0.9 (1)	0.62	3704	} 3725	} 1.63(20)
3717	1.0 (1)	0.69	3717		
3719	0.7 (1)	0.48	3719		
3851	0.4 (1)	0.30	3851	3850	0
3884	0.3 (1)	0.22	3884	3875	0.047(30)
3915	0.3 (1)	0.46	3915	3925	1.47(14)
3976	0.3 (1)	0.28	3976	3975	0.156(20)
4043	1.5 (1)	0.0	4043	} 4050	} 0.313(30)
4045	0.09 (5)	0.083	4045		
			4100	4100	0.019(5)
			4150	4150	0.012(8)
4200[b]		0.092	4200	4200	0.078(20)
			4250	4250	0.127(60)
			4300	4300	0.19(10)

[a]No uncertainties given except for g.s to g.s transition in the original work.
[b]Marked as a "pseudolevel" in original work, which is equivalent to bin in MTAS analysis.

C. Deduced β feeding patterns in ^{142}Cs decay

For ^{142}Cs β decay the comparison of energy spectrum measured by MTAS to the simulated MTAS response using decay data listed in the current ENSDF data base [48] is shown in Fig. 4. The ground-state to ground-state β transition is a first forbidden nonunique decay, $0^- \to 0^+$. The lower β-feeding for the lowest energy states in ^{142}Ba, the ground state and the first excited 2^+ state at 360 keV, is deduced from MTAS measurement. The ^{142}Cs β feeding to the ^{142}Ba ground state is smaller than 56% listed in ENSDF [48] and amounts to 40.6(20)%. For the β feeding to the first excited 2^+ state the upper limit is 0.07(6)%, which is much lower than the previously reported nonzero feeding 7.2(12)% [48].

In ^{142}Cs, β-delayed neutron emission is energetically possible. The ENSDF adopted value of $P_n = 0.0896(36)\%$ follows the result and assessment presented at Ref. [58], in agreement with the values obtained in Refs. [59–61] and rejecting earlier measurements of $P_n = 0.285(26)\%$ [62] and of $0.27(7)\%$ [63]. In this work, we identified a small effect corresponding to the β-delayed neutrons emitted from ^{142}Cs just below 7 MeV in the total MTAS energy spectrum shown in Fig. 4. Using the neutron efficiency of 0.3 ± 0.1 from [15] for neutrons below 200 keV, along with 543(44) counts after background subtraction representing the β-delayed neutrons emitted from ^{142}Cs in the neutron peak around 7 MeV, we obtained the $P_n = 0.10^{+5}_{-3}$ % supporting the recent average value.

The calculated β-feeding intensities using the MTAS data and the simulated responses to each decay path are compared with the ENSDF results [48] using 200 keV bins in Fig. 19. As can be expected for a β decay with a large decay energy of 7.3 MeV, new β-fed levels at higher excitation energies are present resulting in the modification of the β-feeding pattern, decay heat and the properties of emitted antineutrinos. The tabulated β-feeding intensities are given in Table VIII.

VI. DECAY HEAT RELEASE AND ANTINEUTRINO EMISSION

As shown in Table IV, fission products at the $A = 142$ decay chain have high cumulative yields in the thermal neutron induced fission of the main nuclear fuel component ^{235}U. Even small improvements to decay, heat values help estimate better the time profile of γ energy release during the nuclear fuel cycle and after planned or accidental stopping of the power reactor.

After the deconvolution of the MTAS spectra, the average γ energy emitted per β-decay $< E_\gamma >$ can be calculated. The $< E_\gamma >$ per decay for ^{142}La, ^{142}Ba, and ^{142}Cs decay derived from MTAS measurement is compared to the ENSDF and Greenwood data in Table V.

For the isobars with lower β-decay energy, ^{142}Ba and ^{142}La, the differences in the decay heat release between MTAS and earlier tabulated data are not significant, while the change in the ^{142}Cs decay heat is a factor 2.6, representing a large modification of the γ energy release at short times after the fission event.

TABLE VIII. β-feeding intensities for ^{142}Cs $\to$ ^{142}Ba decay. ENSDF data taken from [48]. $< E_{\text{bin}} >$ represents the center of the ^{142}Ba excitation energy bin 100 keV wide taken into account during MTAS data analysis.

E_{level} (keV)	$I_\beta(\%)$ ENSDF	$< E_{\text{bin}} >$	$I_\beta(\%)$ MTAS
0	56(5)		40.6(20)
359.6	7.2(12)		0.07(6)
834.8	–		–
1292.2	–		–
1326.5	19.8(22)		16.9(10)
1423.1	1.9(2)		–
1535.5	4.3(5)		3.3(2)
1639.6	2.0(2)		0.77(40)
1693.0	0.5(10)		–
1781.5	0.46(11)		0.3(2)
2127.9	0.52(6)		0.5(1)
2341.8	1.5(2)		2.1(3)
2569.8	0.5(1)		1.1(2)
2882.6	0.17(12)		2.0(2)
3144.4	0.6(1)		1.79(15)
3261.7	0.5(1)	} 3275	} 3.0(3)
3283.3	1.3(2)		
3573.1	1.0(1)	3500	3.0(3)
–	–	3700	0.2(2)
–	–	3800	4.0(4)
–	–	4000	2.7(3)
–	–	4100	2.0(3)
–	–	4300	1.4(2)
4369.3	0.4(1)	4400	4.0(4)
–	–	4500	1.7(2)
–	–	4600	2.4(2)
–	–	4700	1.1(2)
–	–	4800	0.80(15)
–	–	4900	0.6(1)
–	–	5000	0.5(1)
–	–	5100	0.39(8)
–	–	5200	0.36(8)
5280.4	0.8(1)	5300	0.25(8)
–	–	5400	0.24(8)
–	–	5500	0.5(1)
–	–	5600	0.17(6)
–	–	5700	0.16(6)
–	–	5800	0.17(6)
–	–	5900	<0.06
–	–	6000	0.13(4)
–	–	6100	<0.1
–	–	6200	$0.10^{+0.05}_{-0.03}$
–	–	6300	<0.1
–	–	6400	<0.1
–	–	6500	<0.1
–	–	6600	<0.1
–	–	6700	<0.1
–	–	6800	<0.1
–	–	6900	<0.1
–	–	7000	<0.1
–	–	7100	<0.1
–	–	7200	<0.1
–	–	7300	<0.1

Another impact of MTAS measurements of the mass $A = 142$ isobars is on the evaluated cross section for detecting via inverse-β decay reactor antineutrinos associated with [142]La and [142]Cs decays in units of 10^{-43} cm^2. The previous decay properties for [142]La assessed with the ENSDF data base [48] give the value of 0.403, while MTAS measurement reduces this value by about 8%, to 0.373 (22). For [142]Cs, the change is larger. The 7.0(5) value calculated basing on the ENSDF entry is reduced by 27% to 5.1(2) after the MTAS measurement [13,14]. Note that the magnitude of the so called reactor antineutrino anomaly is at the level of 5% [3], so even the [142]La change is significant. [142]Ba has too low of a Q$_\beta$ to affect the reactor antineutrino anomaly.

VII. SUMMARY

New results have been obtained on the β decays of the $A = 142$ isobars [142]La, [142]Ba, and [142]Cs using Oak Ridge National Laboratory's (ORNL) Modular Total Absorption Spectrometer (MTAS) at the ORNL mass separator on-line to the Tandem Accelerator. MTAS is a powerful total absorption spectrometer designed to study complex decays of fission products, with its superior active volume and modularity allowing for advanced analysis of decay path patterns. The studied $A = 142$ isobars have high cumulative fission yields for nuclear fuel components, σ_{cum} up to ∼6%, and therefore contribute to decay heat and antineutrino production at power reactors, see the recent summation analysis [64]. MTAS spectra analysis slightly corrected data content (ENSDF, ENDF) for the decay of [142]Ba with a low-Q_β value of 2.2 MeV. For the žmid range Q_β value of 4.5 MeV for [142]La decay, MTAS analysis allows us to correct the β-feeding pattern (e.g., the feeding to the 1st excited state and the ground state to ground state feeding), with respect to the previous high energy resolution studies and earlier TAS results from Greenwood [43]. Half-lives of the $A = 142$ isobars are improved, demon-strating the potential of high efficiency MTAS array to obtain accurate and precise nuclear data. Due to the large counting statistics, improvements by factors of 5 and 2 to the [142]La and [142]Cs half-lives precision are made, respectively. The results include β-delayed neutron branching ratio $P_n = 0.10^{+5}_{-3}$ % for [142]Cs emitter deduced from MTAS energy spectrum. MTAS data lower the number of antineutrinos emitted from the [142]La and interacting with detector matter by about 8%. The fission product [142]La ($T_{1/2} = 91.1$ min), and [88]Rb ($T_{1/2} = 17.8$ min) presented earlier [17], were recently found out to be among important activities for the analysis of the antineutrino energy spectra after the Double Chooz reactors shutdown [65]. For the [142]Cs further away from stability, with higher Q_β value about 7.3 MeV, the changes after MTAS results are significant and of high importance for reactor decay heat release at short times after fission event. The flux of reactor antineutrinos interacting with matter is lowered by as much as 27% for [142]Cs and due to its large cumulative fission yields, this is a major correction. In addition to these major corrections for the [142]Cs decay pattern [13,14], the corrections to [142]Ba and [142]La decay patterns and their impacts on decay heat and detected reactor antineutrinos are also reported.

[1] https://pris.iaea.org/pris/.

[2] M. Gospodarczyk (2021), https://www.iaea.org/newscenter/news/nuclear-power- proves-its-vital-role-as-an-adaptable-reliable -supplier-of-electricity-during-covid-19.

[3] D. Adey, F. P. An, A. B. Balantekin, H. R. Band, M. Bishai, S. Blyth, D. Cao, G. F. Cao, J. Cao, J. F. Chang *et al.* (Daya Bay Collaboration), Phys. Rev. Lett. **123**, 111801 (2019).

[4] J. K. Ahn, S. Chebotaryov, J. H. Choi, S. Choi, W. Choi, Y. Choi, H. I. Jang, J. S. Jang, E. J. Jeon, I. S. Jeong *et al.* (RENO Collaboration), Phys. Rev. Lett. **108**, 191802 (2012).

[5] Y. Abe, J. C. Anjos, J. C. Barriere, E. Baussan, I. Bekman, M. Bergevin, T. J. C. Bezerra, L. Bezrukov, E. Blucher, C. Buck *et al.*, J. High Energy Phys. 10 (2014) 086.

[6] G. Mention, M. Fechner, T. Lasserre, T. A. Mueller, D. Lhuillier, M. Cribier, and A. Letourneau, Phys. Rev. D **83**, 073006 (2011).

[7] F. An, G. An, Q. An, V. Antonelli, E. Baussan, B. J., L. Bezrukov, S. Blyth, R. Brugnera, M. Buizza Avanzini *et al.*, J. Phys. G: Nucl. Part. Phys. **43**, 030401 (2016).

[8] A. A. Sonzogni, M. Nino, and E. A. McCutchan, Phys. Rev. C **98**, 014323 (2018).

[9] L. Zhang, Y. Wang, J. Cao, and L. Wen, Phys. Rev. D **79**, 073007 (2009).

[10] A. Ashenfelter, B. Balantekin, C. Baldenegro, H. Band, C. Bass, D. Bergeron, D. Berish, L. Bignell, N. Bowden, J. Boyle *et al.* (PROSPECT Collaboration), Nucl. Instrum. Methods Phys. Res., Sec. A **922**, 287 (2019).

[11] J. Ashenfelter, A. B. Balantekin, H. R. Band, C. D. Bass, D. E. Bergeron, D. Berish, N. S. Bowden, J. P. Brodsky, C. D. Bryan, J. J. Cherwinka *et al.* (PROSPECT Collaboration), Phys. Rev. Lett. **122**, 251801 (2019).

[12] A. Bernstein, N. Bowden, B. Goldblum, P. Huber, I. Jovanovic, and J. Mattingly, Rev. Mod. Phys. **92**, 011003 (2020).

[13] B. C. Rasco, M. Wolińska-Cichocka, A. Fijałkowska, K. P. Rykaczewski, M. Karny, R. K. Grzywacz, K. C. Goetz, C. J. Gross, D. W. Stracener, E. F. Zganjar *et al.*, Phys. Rev. Lett. **117**, 092501 (2016).

[14] A. Fijałkowska, M. Karny, K.P. Rykaczewski, B.C. Rasco, R. Grzywacz, C.J. Gross, M. Wolinska-Cichocka, K.C. Goetz, D.W. Stracener, W. Bielewski, R. Goans, J.H. Hamilton, J.W. Johnson, C. Jost, M. Madurga, K. Miernik, D. Miller, S.W.

Padgett, S.V. Paulauskas, A.V. Ramayya, and E.F. Zganjar, Phys. Rev. Lett. **119**, 052503 (2017).

[15] B. C. Rasco, K. P. Rykaczewski, A. Fijałkowska, M. Karny, M. Wolińska-Cichocka, R. K. Grzywacz, C. J. Gross, D. W. Stracener, E. F. Zganjar, J. C. Blackmon *et al.*, Phys. Rev. C **95**, 054328 (2017).

[16] B. C. Rasco, K. P. Rykaczewski, A. Fijalkowska, M. Karny, M. Wolinska-Cichocka, R. K. Grzywacz, D. W. Stracener, E. F. Zganjar, J. C. Batchelder, J. C. Blackmon, N. T. Brewer, M. P. Cooper, K. C. Goetz, J. W. Johnson, T. King, A. Laminack, J. T. Matta, K. Miernik, M. Madurga, D. Miller, M. M. Rajabali, T. Ruland, P. Shuai, M. Stepaniuk, and J. Winger, Phys. Rev. C **105**, 064301 (2022).

[17] P. Shuai, B. C. Rasco, K. P. Rykaczewski, A. Fijałkowska, M. Karny, M. Wolińska-Cichocka, R. K. Grzywacz, C. J. Gross, D. W. Stracener, E. F. Zganjar *et al.*, Phys. Rev. C **105**, 054312 (2022).

[18] A. L. Nichols, J. Nucl. Sci. Technol. **52**, 17 (2015).

[19] T. Yoshida, A. L. Nichols, M. A. Kellett, O. Bersillon, H. Henriksson, R. Jacqmin, B. Roque, J. Katakura, K. Oyamatsu, T. Tachibana *et al.*, *Assessment of Fission Product Decay Data for Decay Heat Calculations: A report by the Working Party on International Evaluation Co-operation of the Nuclear Energy Agency Nuclear Science Committee* (Nuclear Energy Agency, Organization for Economic Co-operation and Development, Paris, France, 2007), Vol. 25.

[20] A. A. Sonzogni, T. D. Johnson, and E. A. McCutchan, Phys. Rev. C **91**, 011301(R) (2015).

[21] D. A. Dwyer and T. J. Langford, Phys. Rev. Lett. **114**, 012502 (2015).

[22] J. C. Hardy, L. C. Carraz, B. Jonson, and P. G. Hansen, Phys. Lett. B **71**, 307 (1977).

[23] C. L. Duke, P. G. Hansen, O. B. Nielson, G. Rudstam, and the ISOLDE Collaboration, Nucl. Phys. A **151**, 609 (1970).

[24] P. Hornshøj, B. R. Erdal, P. G. Hansen, B. Jonson, K. Aleklett, and G. Nyman, Nucl. Phys. A **239**, 15 (1975).

[25] A. Bykov, V. Vitman, F. Moroz, and Y. Naumov, Izv. Akad. Nauk SSSR, Ser. Fiz **44**, 918 (1980).

[26] R. C. Greenwood, R. G. Helmer, M. A. Lee, M. H. Putnam, M. A. Oates, D. A. Struttmann, and K. D. Watts, Nucl. Instrum. Methods Phys. Res., Sec. A **314**, 514 (1992).

[27] M. Karny, J. Nitschke, L. Archambault, K. Burkard, D. Cano-Ott, M. Hellström, W. Hüller, R. Kirchner, S. Lewandowski, E. Roeckl *et al.*, Nucl. Instrum. Methods Phys. Res. Sec. B **126**, 411 (1997).

[28] B. Rubio, W. Gelletly, E. Nácher, A. Algora, J. Taín, A. Perez, and L. Caballero, J. Phys. G: Nucl. Part. Phys. **31**, S1477 (2005).

[29] J. L. Taín, International Conference on Nuclear Data for Science and Technology, 2007.

[30] E. Valencia, J. L. Tain, A. Algora, J. Agramunt, E. Estevez, M. D. Jordan, B. Rubio, S. Rice, P. Regan, W. Gelletly, Z. Podolyak, M. Bowry, P. Mason, G. F. Farrelly, A. Zakari-Issoufou, M. Fallot, A. Porta, V. M. Bui, J. Rissanen, T. Eronen, I. Moore, H. Penttila, J. Aysto, V. V. Elomaa, J. Hakala, A. Jokinen, V. S. Kolhinen, M. Reponen, V. Sonnenschein, D. Cano-Ott, A. R. Garcia, T. Martinez, E. Mendoza, R. Caballero-Folch, B. Gomez-Hornillos, V. Gorlichev, F. G. Kondev, A. A. Sonzogni, and L. Batist, Phys. Rev. C **95**, 024320 (2017).

[31] A. Simon, S. Quinn, A. Spyrou, A. Battaglia, I. Beskin, A. Best, B. Bucher, M. Couder, P. DeYoung, X. Fang *et al.*, Nucl. Instrum. Methods Phys. Res., Sect. A **703**, 16 (2013).

[32] J. Taín, A. Algora, J. Agramunt, V. Guadilla, D. Jordan, A. Montaner-Pizá, B. Rubio, E. Valencia, D. Cano-Ott, W. Gelletly *et al.*, Nucl. Instrum. Methods Phys. Res., Sect. A **803**, 36 (2015).

[33] V. Guadilla, J. Taín, A. Algora, J. Agramunt, J. Äystö, J. Briz, A. Cucoanes, T. Eronen, M. Estienne, M. Fallot *et al.*, Nucl. Instrum. Methods Phys. Res., Sect. A **910**, 79 (2018).

[34] A. Algora, J. L. Tain, B. Rubio, M. Fallot, and W. Gelletly, Eur. Phys. J. A **57**, 85 (2021).

[35] M. Wolińska-Cichocka, K. P. Rykaczewski, A. Fijałkowska, M. Karny, R. K. Grzywacz, J. Gross, C. J. Johnson, B. C. Rasco, and E. F. Zganjar, Nucl. Data Sheets **120**, 22 (2014).

[36] K. P. Rykaczewski, Nucl. Data Sheets **120**, 16 (2014).

[37] B. C. Rasco, A. Fijałkowska, M. Karny, K. P. Rykaczewski, M. Wolińska-Cichocka, R. Grzywacz, and K. C. Goetz, Nucl. Instrum. Methods Phys. Res., Sect. A **788**, 137 (2015).

[38] M. Karny, K. P. Rykaczewski, A. Fijałkowska, B. C. Rasco, M. Wolińska-Cichocka, R. K. Grzywacz, K. C. Goetz, D. Miller, and E. F. Zganjar, Nucl. Instrum. Methods Phys. Res., Sect. A **836**, 83 (2016).

[39] M. Wolińska-Cichocka, B. Rasco, K. Rykaczewski, N. Brewer, D. Stracener, R. Grzywacz, C. Gross, A. Fijałkowska, K. Goetz, M. Karny *et al.*, EPJ Web Conf. **146**, 10005 (2017).

[40] S. L. Tong, W. V. Prestwitch, and K. Fritze, Can. J. Phys. **49**, 1179 (1971).

[41] J. T. Larsen, W. L. Talbert, and J. R. McConnell, Phys. Rev. C **3**, 1372 (1971).

[42] C. Chung, W. B. Walters, D. S. Brenner, A. Aprahamian, R. L. Gill, M. Shmid, R. E. Chrien, L. J. Yuan, A. Wolf, and Z. Berant, Phys. Rev. C **28**, 2099 (1983).

[43] R. C. Greenwood, R. G. Helmer, M. H. Putnam, and K. D. Watts, Nucl. Instrum. Methods Phys. Res., Sect. A **390**, 95 (1997).

[44] J. R. Beene, D. W. Bardayan, A. Galindo Uribarri, C. Gross, K. L. Jones, J. F. Liang, W. Nazarewicz, D. W. Stracener, B. A. Tatum, and R. L. Varner, J. Phys. G: Nucl. Part. Phys. **38**, 024002(2011).

[45] D. Stracener, Nucl. Instrum. Methods Phys. Res., Sect. B **204**, 42 (2003), 14th International Conference on Electromagnetic Isotope Separators and Techniques Related to their Applications.

[46] R. Grzywacz, Nucl. Instrum. Methods Phys. Res., Sect. B **204**, 649 (2003).

[47] R. Grzywacz, C. Gross, A. Korgul, S. Liddick, C. Mazzocchi, R. Page, and K. Rykaczewski, Nucl. Instrum. Methods Phys. Res., Sect. B **261**, 1103 (2007).

[48] T. Johnson, D. Symochko, M. Fadil, and J. Tuli, Nucl. Data Sheets **112**, 1949 (2011).

[49] F. Krishichayan, M. Bhike, C. R. Howell, A. P. Tonchev, and W. Tornow, Phys. Rev. C **100**, 014608 (2019).

[50] M. Wang, W. J. Huang, F. G. Kondev, G. Audi, and S. Naimi, Chinese Phys. C **45**, 2021 (030003).

[51] B. C. Rasco, A. Fijałkowska, M. Karny, K. Rykaczewski, M. Wolińska-Cichocka, K. C. Goetz, R. K. Grzywacz, C. J. Gross, K. Miernik, and S. V. Paulauskas, JPS Conf. Proc. **6**, 030018 (2015).

[52] J. Allison, K. Amako, J. Apostolakis, H. Araujo, P. Dubois, M. Asai, G. Barrand, R. Capra, S. Chauvie, R. Chytracek *et al.*, Nuclear Science, IEEE Transactions on **53**, 270 (2006).

[53] B. C. Rasco, A. Fijałkowska, K. P. Rykaczewski, M. Wolińska-Cichocka, M. Karny, R. K. Grzywacz, K. C. Goetz, C. J. Gross, D. W. Stracener *et al.*, Acta Phys. Pol. B **48**, 507 (2017).

[54] M. Chadwick, M. Herman, P. ObloŽinský, M. Dunn, Y. Danon, A. Kahler, D. Smith, B. Pritychenko, G. Arbanas, R. Arcilla *et al.*, Nucl. Data Sheets **112**, 2887 (2011).

[55] A. Mattera and A. A. Sonzogni, Report BNL-220804-2021-INRE (2021).

[56] https://www.oecd-nea.org/dbdata/jeff/jeff33/index.html.

[57] R. Mills, EPJ Web Conf. **146**, 04008 (2017).

[58] G. Rudstam, K. Aleklett, and L. Sihver, At. Data Nucl. Data Tables **53**, 1 (1993).

[59] P. L. Reeder and R. Warner, Delayed Neutron Emission Probabilities of Rb and Cs Precursors Measured by Both Ion and Beta Counting Techniques, Research Report **PNL-SA-8766**, Pacific Northwest Laboratories (1980).

[60] E. Lund, P. Hoff, K. Aleklett, O. Glomset, and G. Rudstam, Z. Phys. A **294**, 233 (1980).

[61] G. Engler and E. Ne'eman, Nucl. Phys. A **367**, 29 (1981).

[62] M. Asghar, J. Crançon, J. Gautheron, and C. Ristori, J. Inorg. Nucl. Chem. **37**, 1563 (1975).

[63] W. L. Talbert Jr., A. B. Tucker, and G. M. Day, Phys. Rev. **177**, 1805 (1969).

[64] M. Estienne, M. Fallot, A. Algora, J. Briz-Monago, V. M. Bui, S. Cormon, W. Gelletly, L. Giot, V. Guadilla, D. Jordan *et al.*, Phys. Rev. Lett. **123**, 022502 (2019).

[65] A. Onillon, contribution to IAEA Technical Meeting, 16th-20th January 2023, Vienna, Austria **IAEA** (2023).